Research Article

Journal of Molecular Recognition

Received: 25 April 2013, Revised: 25 June 2013, Accepted: 26 June 2013, Published online in Wiley Online Library

(wileyonlinelibrary.com) DOI: 10.1002/jmr.2295

Biophysical basis of the promiscuous binding of B-cell lymphoma protein 2 apoptotic repressor to BH3 ligands

Vikas Bhat, Max B. Olenick, Brett J. Schuchardt, David C. Mikles, Caleb B. McDonald and Amjad Farooq*

B-cell lymphoma protein 2 (Bcl2) apoptotic repressor carries out its function by virtue of its ability to bind to BH3 domains of various pro-apoptotic regulators in a highly promiscuous manner. Herein, we investigate the biophysical basis of such promiscuity of Bcl2 toward its cognate BH3 ligands. Our data show that although the BH3 ligands harboring the LXXXAD motif bind to Bcl2 with submicromolar affinity, those with the LXXX[G/S]D motif afford weak interactions. This implies that the replacement of alanine at the fourth position (A + 4)—relative to the N-terminal leucine (L0) within the LXXXAD motif—to glycine/serine results in the loss of free energy of binding. Consistent with this notion, the A + 4 residue within the BH3 ligands harboring the LXXXAD motif engages in key intermolecular van der Waals contacts with A149 lining the ligand binding groove within Bcl2, whereas A + 4G/S substitution results in the disruption of such favorable binding interactions. Of particular interest is the observation that although increasing ionic strength has little or negligible effect on the binding of high-affinity BH3 ligands harboring the LXXXAD motif, the binding of those with the LXXX[G/S]D motif in general experiences a varying degree of enhancement. This salient observation is indicative of the fact that hydrophobic forces not only play a dominant but also a universal role in driving the Bcl2-BH3 interactions. Taken together, our study sheds light on the molecular basis of the factors governing the promiscuous binding of Bcl2 to pro-apoptotic regulators and thus bears important consequences on the development of rational therapeutic approaches. Copyright © 2013 John Wiley & Sons, Ltd.

Keywords: binding thermodynamics; salt dependence; structural models; molecular dynamics

INTRODUCTION

One of the key players involved in mediating the apoptotic fate of cells during physiological processes such as embryonic development and cellular homeostasis is the Bcl2 family of proteins (Adams and Cory, 1998; Gross *et al*., 1999; Korsmeyer, 1999; Kuwana and Newmeyer, 2003; Dewson and Kluck, 2009; Chipuk *et al*., 2010; Dejean *et al*., 2010). Briefly, the Bcl2 proteins can be divided into three major groups with respect to their role in the regulation of apoptotic machinery: activators, effectors, and repressors (Figure 1a). In a nutshell, the apoptotic fate, or the decision of a cell to live or die, is determined by the cellular ratio of activator, effector, and repressor molecules (Chipuk and Green, 2008; Chipuk *et al*., 2008). In quiescent and healthy cells, the effectors are maintained in an inactive state via complexation with repressors. Upon receiving apoptotic cues, in the form of DNA damage and cellular stress, the activators are stimulated and compete with effectors for binding to the repressors and, in so doing, not only do they neutralize the anti-apoptotic action of repressors but also unleash the pro-apoptogenicity of effectors.

The effectors subsequently initiate apoptotic cell death by virtue of their ability to insert into the mitochondrial outer membrane resulting in the formation of mitochondrial pores in a manner akin to the insertion of bacterial toxins such as colicins and diphtheria (van der Goot *et al*., 1991; London, 1992; Lakey *et al*., 1994; Schendel *et al*., 1998; Zakharov and Cramer, 2002). This leads to the release of apoptogenic factors such as cytochrome c and Smac/Diablo from mitochondria into the cytosol. Subsequently, rising levels of apoptogenic factors in the cytosol switch on aspartate-specific proteases termed caspases, which in turn, demolish the cellular architecture by cleavage of proteins culminating in total cellular destruction. In this manner, the concerted action of various Bcl2 proteins keeps apoptosis in check in a healthy cell, while their dysregulation is met with serious pathological consequences. In particular, overexpression of

* *Correspondence to: A. Farooq, Department of Biochemistry & Molecular Biology, Miller School of Medicine, University of Miami, Miami, FL 33136, USA. E-mail: amjad@farooqlab.net*

V. Bhat, M. B. Olenick, B. J. Schuchardt, D. C. Mikles, C. B. McDonald, A. Farooq Department of Biochemistry & Molecular Biology, Miller School of Medicine, University of Miami, Miami, FL 33136, USA

Abbreviations: *Bad, Bcl2-associated death promoter; Bak, Bcl2-homologous antagonist/killer; Bax, Bcl2-associated protein X; Bcl2, B-cell lymphoma protein 2; BclW, Bcl2-like protein 2; BclXL, B-cell lymphoma extra-large protein; Bfl1, Bcl2-related protein A1; Bid, BH3-interacting domain death agonist; Bik, Bcl2-interacting killer; Bim, Bcl2-interacting mediator; Bmf, Bcl2-modifying factor; Hrk, harakiri apoptotic activator; ITC, isothermal titration calorimetry; LIC, ligation-independent cloning; Mcl1, myeloid leukemia cell protein 1; MD, molecular dynamics; MM, molecular modeling; MOM, mitochondrial outer membrane; Noxa, phorbol-induced protein 1; Puma, p53-upregulated modulator of apoptosis; SASA, solvent-accessible surface area; SEC, size-exclusion chromatography; TM, transmembrane (TM) domain.*

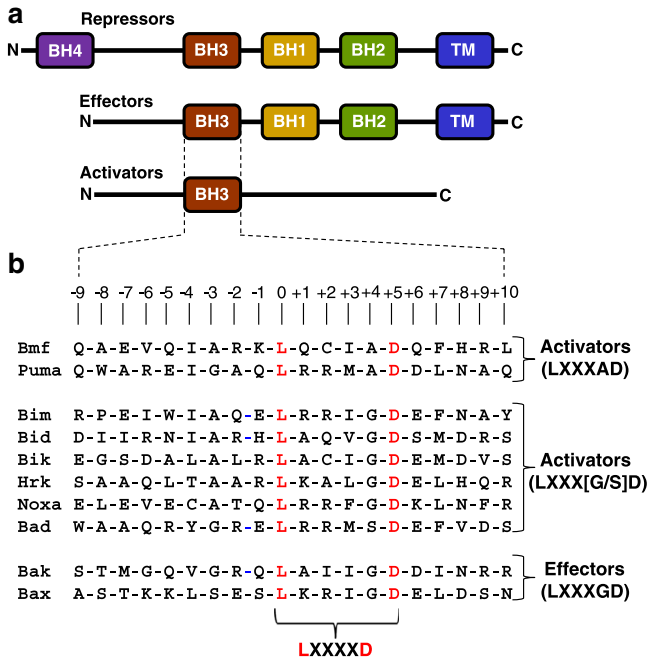

Figure 1. An overview of B-cell lymphoma protein 2 (Bcl2) family of proteins. (a) Structural organization of pro-survival (repressors) and pro-apoptotic (effectors and activators) regulators. The activators belong to the BH3-only proteins, where BH3 is the Bcl2 homology three domain. Examples of activators include Bcl2-associated death promoter, BH3 interacting domain death agonist, Bcl2-interacting killer, Bcl2-interacting mediator, Bcl2-modifying factor, harakiri apoptotic activator, phorbol-induced protein 1, and p53-upregulated modulator of apoptosis. The effectors contain the BH3-BH1-BH2-TM modular architecture, where TM is the transmembrane domain located C-terminal to Bcl2 homology domains BH3, BH1, and BH2. Examples of effectors are Bcl2-homologous antagonist/killer and Bcl2-associated protein X. The repressors are usually characterized by the BH4-BH3-BH1-BH2-TM modular organization, with an additional N-terminal Bcl2 homology four domain. Examples of repressors are Bcl2, BclXL, BclW, Mcl1, and Bfl1. (b) Amino acid sequence alignment of BH3 domains of various activators and effectors encoded by the human genome and employed in this study as ligands for Bcl2. Note that the absolutely conserved consensus leucine and aspartate residues within the LXXXXD motif shared by all BH3 domains are colored red. The numerals indicate the nomenclature used in this study to distinguish residues within and flanking the core LXXXXD motif relative to the consensus leucine, which is arbitrarily assigned zero.

apoptotic repressors such as Bcl2 and BclXL in healthy tissues is associated with the development of various cancers (Del Bufalo *et al*., 1997; Espana *et al*., 2004; Placzek *et al*., 2010).

Although there is a general consensus that hetero-association between various members of the Bcl2 family represents a defining event in the decision of a cell to live or die, the molecular basis of such protein–protein interactions remains hitherto poorly characterized. In particular, the BH3 domain of pro-apoptotic regulators such as activators and effectors—typically about 20 amino acids in length and characterized by the presence of the core LXXXXD motif (Figure 1b)—has risen to prominence for its key role in mediating apoptosis on at least two major fronts. First, the repressors unleash their anti-apoptotic action by virtue of their ability to bind to the BH3 domain of effectors. Second, the activators initiate apoptosis by virtue of the ability of their BH3 domains to compete with the BH3 domains of effectors for binding to repressors and, in so doing, drive the apoptotic machinery by neutralizing the repressors.

Despite such a critical role of BH3 domains of activators and effectors in mediating apoptosis, the molecular basis of their binding specificity largely remains obscure. In an effort to fill this void in our knowledge, we employ here various biophysical tools to investigate the molecular basis of the binding promiscuity of Bcl2 apoptotic repressor toward its cognate BH3 ligands. Herein, we show that the various BH3 ligands can be dissected into two distinct classes harboring the LXXXAD and LXXX[G/S]D motifs on the basis of their binding characteristics to Bcl2. Our detailed biophysical analysis sheds new light on the mechanism of Bcl2-ligand recognition.

MATERIALS AND METHODS

Sample preparation

Human Bcl2 (residues 1–205), devoid of the C-terminal region (residues 206–239) harboring the TM domain, was cloned into pET30 bacterial expression vectors with an N-terminal His-tag using Novagen LIC technology (Novagen, Madison, WI, USA). The recombinant protein was subsequently expressed in Escherichia coli BL21* (DE3) bacterial strain (invitrogen) and purified on a Ni-NTA affinity column using standard procedures. Briefly, bacterial cells were grown at 20 °C in Terrific Broth to an optical density of greater than unity at 600 nm prior to induction with 0.5 mM isopropyl β-D-1-thiogalactopyranoside. The bacterial culture was further grown overnight at 20 °C, and the cells were subsequently harvested and disrupted using a BeadBeater (Biospec) (Biospec, Bartlesville, OK, USA). After separation of cell debris at high-speed centrifugation, the cell lysate was loaded onto a Ni-NTA column and washed extensively with 20 mM imidazole to remove non-specific binding of bacterial proteins to the column. The recombinant protein was eluted with 200 mM imidazole and dialyzed against an appropriate buffer to remove excess imidazole. Further treatment on a Hiload Superdex 200 size-exclusion chromatography column coupled in-line with GE Akta FPLC system (GE Healthcare, Milwaukee, WI, USA) led to purification of Bcl2 to an apparent homogeneity as judged by SDS-PAGE analysis. Final yield was typically between 5–10 mg protein of apparent homogeneity per liter of bacterial culture. Protein concentration was determined by the fluorescence-based Quant-It assay (invitrogen) and spectrophotometrically using an extinction coefficients of 37 930/M/cm calculated using the online software ProtParam at ExPasy Server (Invitrogen, Carlsbad, CA, USA) (Gasteiger *et al*., 2005). Results from both methods were in an excellent agreement. We note here that the purification of full-length construct of Bcl2 (residues 1–239) has not hitherto been achieved by any laboratory—largely because of the hydrophobic nature of the C-terminal TM domain—and that, despite our repeated attempts, nor were we able to purify the fully intact Bcl2 to sufficient quantities and an apparent homogeneity required for biophysical analysis. The 20-mer wildtype and mutant peptides spanning the BH3 domains from various human apoptotic effectors and activators were commercially obtained from GenScript Corporation. The amino acid sequence of wildtype BH3 peptides employed in this study is provided in Figure 1b. The concentration of all BH3 peptides was measured gravimetrically.

Isothermal titration calorimetry

Isothermal titration calorimetry experiments were performed on a Microcal VP-ITC instrument (Microcal, Springfield, MA, USA). Briefly,

Bcl2 and various BH3 peptides were pre-dialyzed in 50 mM sodium phosphate buffer containing 0–500 mM NaCl, 1 mM EDTA, and 5 mM β-mercaptoethanol at pH 7.0. ITC experiments were initiated by injecting 25 x 10 μl aliquots of 1–2 mM of each BH3 peptide from the syringe into the calorimetric cell containing 25–50 μM of 1.46 ml of Bcl2 at various temperatures in the 15–35 °C range. In each case, the change in thermal power as a function of each injection was automatically recorded using the ORIGIN software (Microcal Origin, Northampton, MA, USA), and the raw data were further processed to yield binding isotherms of heat release per injection as a function of molar ratio of each BH3 peptide to Bcl2. The heats of mixing and dilution were subtracted from the heats of binding per injection by carrying out a control experiment in which the same buffer in the calorimetric cell was titrated against each BH3 peptide in an identical manner. The apparent equilibrium dissociation constant (K_d) and the enthalpic change (ΔH) associated with peptide binding to Bcl2 were determined from the non-linear least-squares fit of data to a one-site binding model as described previously (Wiseman *et al*., 1989; Bhat *et al*., 2012). The binding free energy change (ΔG) was calculated from the following expression:

$$\Delta G = RT\ln K_d \quad (1)$$

where R is the universal molar gas constant (1.99 cal/K/mol) and T is the absolute temperature. The entropic contribution ($T\Delta S$) to the free energy of binding was calculated from the relationship:

$$T\Delta S = \Delta H - \Delta G \quad (2)$$

where ΔH and ΔG are as defined previously. Heat capacity change (ΔC_p) and enthalpy change at 60 °C (ΔH_{60}) associated with peptide binding to Bcl2 were determined from the slopes and y-extrapolations to a temperature of 60 °C of $\Delta H-T$ plots, respectively. Changes in SASA upon the binding of various BH3 peptides to Bcl2 were subsequently calculated from the experimentally determined values of ΔC_p and ΔH_{60}. To determine changes in polar SASA ($\Delta SASA_{polar}$) and apolar SASA ($\Delta SASA_{apolar}$) upon peptide binding to Bcl2, it was assumed that ΔC_p and ΔH_{60} are additive and linearly depend on the change in $\Delta SASA_{polar}$ and $\Delta SASA_{apolar}$ as embodied in the following empirically derived expressions (Murphy and Freire, 1992; Spolar and M.T. Record, 1994; Xie and Freire, 1994; Edgcomb and Murphy, 2000):

$$\Delta C_p = a\left[\Delta SASA_{polar}\right] + b\left[\Delta SASA_{apolar}\right] \quad (3)$$

$$\Delta H_{60} = c\left[\Delta SASA_{polar}\right] + d\left[\Delta SASA_{apolar}\right] \quad (4)$$

where a, b, c, and d are empirically determined coefficients with values of −0.14 cal/mol/K/Å^2, +0.32 cal/mol/K/Å^2, +31.34 cal/mol/Å^2 and −8.44 cal/mol/Å^2, respectively. The coefficients a and b are independent of temperature, whereas c and d refer to a temperature of 60 °C, which equates to the median melting temperature of the proteins from which these constants are derived (Murphy and Freire, 1992; Xie and Freire, 1994; Edgcomb and Murphy, 2000). With ΔC_p and ΔH_{60} experimentally determined using ITC and the knowledge of coefficients a–d from empirical models (Murphy and Freire, 1992; Spolar and M.T. Record, 1994; Xie and Freire, 1994; Edgcomb and Murphy, 2000), Eqs [3] and [4] were simultaneously solved to obtain the magnitudes of $\Delta SASA_{polar}$ and $\Delta SASA_{apolar}$. Total change in SASA ($\Delta SASA_{total}$) is defined by the following equation:

$$\Delta SASA_{total} = \Delta SASA_{polar} + \Delta SASA_{apolar} \quad (5)$$

Molecular modeling

Molecular modeling was employed to build structural models of Bcl2 (residues 1–205) in complex with 20-mer BH3 peptides harboring LXXXAD (Puma), LXXXGD (Bax), and LXXXSD (Bad) motifs using the MODELLER software (University of California, San Francisco, CA, USA) based on homology modeling (Marti-Renom *et al*., 2000). Briefly, the structural models were constructed using the experimentally determined structures of Bcl2 in complex with a BH3 peptide derived from Bax (PDB# 2XA0) and BclXL in complex with a BH3 peptide derived from Bad (PDB# 1G5J) in a multi-template alignment fashion. In each case, a total of 100 structural models was calculated, and the structure with the lowest energy, as judged by the MODELLER objective function, was selected for further analysis. The structural models were rendered using RIBBONS (Carson, 1991).

Molecular dynamics

Molecular dynamics simulations were performed with the GROMACS software (Stockholm Center for Biomembrane Research, Stockholm, Sweden) (Van Der Spoel *et al*., 2005; Hess, 2008) using the integrated OPLS-AA force field (Jorgensen and Tirado-Rives, 1988; Kaminski *et al*., 2001). Briefly, the structural models of Bcl2 bound to 20-mer BH3 peptides harboring LXXXAD (Puma), LXXXGD (Bax), and LXXXSD (Bad) motifs were centered within a cubic box with dimensions of 10 Å, hydrated using the extended simple point charge water model (Toukan and Rahman, 1985; Berendsen *et al*., 1987), and the ionic strength of solution was set to 100 mM with NaCl. The hydrated structures were energy-minimized with the steepest descent algorithm prior to equilibration under the NPT ensemble conditions, wherein the number of atoms (N), pressure (P), and temperature (T) within the system were respectively kept constant at ~50 000, 1 bar, and 300 K. The Particle-Mesh Ewald method was employed to compute long-range electrostatic interactions with a 10 Å cut-off (Darden *et al*., 1993) and the Linear Constraint Solver algorithm to restrain bond lengths (Hess *et al*., 1997). All MD simulations were performed under periodic boundary conditions using the leap-frog integrator with a time step of 2 fs. For the final MD production runs, data were collected every 100 ps over a time scale of 100 ns. All simulations were run on a Linux workstation using parallel processors at the High Performance Computing facility within the Center for Computational Science of the University of Miami. Importantly, all MD simulations were repeated at least once and were reproducible with negligible differences in the trajectories in agreement with the fact that GROMACS is based on a deterministic algorithm—a pre-defined set of equations that will always produce the same output for a given system.

RESULTS AND DISCUSSION

Distinct motifs underscore the differential binding of BH3 ligands to B-cell lymphoma protein 2

Unraveling the specificity of BH3 ligands toward Bcl2 and other apoptotic repressors has been an area of immense interest over the past decade or so. Importantly, previous work has shown that residues within and flanking the LXXXXD motif account for the specificity of binding of BH3 ligands to apoptotic repressors (Sattler *et al*., 1997; Huang and Strasser, 2000; Petros *et al*., 2000; Liu *et al*., 2003; Petros *et al*., 2004; Lee *et al*., 2007; Boersma *et al*., 2008; Moroy *et al*., 2009; Yao *et al*., 2009; Dutta *et al*., 2010; Ku *et al*., 2011; London *et al*., 2012). In particular, these studies reveal that in addition to consensus leucine (L0) and aspartate (D + 5) within the LXXXXD motif of BH3 ligands (Figure 1b), the hydrophobic residues at the −4, +3, and +7 positions represent binding "hotspots" that determine the selectivity of molecular recognition by virtue of their ability to align along one face of the amphipathic BH3 α-helix that is accommodated within the hydrophobic groove of apoptotic repressors. In an effort to further build on this work and to understand the ligand specificity of Bcl2, we measured the binding of Bcl2 to BH3 peptides derived from various pro-apoptotic regulators using ITC. Figure 2 shows representative ITC isotherms for the binding of Bcl2 to BH3 peptides of Puma, Bax, and Bad, whereas detailed thermodynamics accompanying such macromolecular associations for all potential BH3 ligands are provided in Table 1.

Our data show that although all BH3 ligands are characterized by the presence of the core LXXXXD motif (Figure 1b), residues within and flanking this motif further buttress the Bcl2-ligand interaction in a predictable fashion. Importantly, the various BH3 ligands of Bcl2 can be divided into two major classes on the basis of whether they harbor the LXXXAD (class I) or the LXXX[G/S]D (class II) motif (Table 1). Of particular note is the observation that the BH3 ligands characterized by these motifs display differential binding to Bcl2. Thus, although BH3 ligands harboring the LXXXAD motif bind to Bcl2 with submicromolar affinities, those harboring the LXXX[G/S]D motif—with the exception of Noxa for which no binding was observed—do so with weaker affinities in the micromolar range. This implies that the replacement of alanine at the fourth position (A + 4)—relative to the N-terminal leucine (L0) within the LXXXAD motif (Figure 1b)—to glycine results in the loss of free energy of binding.

In order to test the validity of this hypothesis further, we next generated various mutant BH3 peptides to probe the effect of appropriate amino acid changes within and flanking the LXXXXD motif and subsequently analyzed their binding to Bcl2 using ITC in a manner akin to that conducted for wildtype BH3 peptides (Table 2). Our analysis reveals that the A + 4G substitution within the Puma peptide (Puma_A + 4G) harboring the high-affinity LXXXAD motif results in the loss of binding affinity to Bcl2 by more than five-fold, implying that the A + 4G replacement within the BH3 ligands harboring the LXXXGD motif indeed accounts for their low-affinity binding to Bcl2. This view is further substantiated by the observation that the G + 4A substitution within the Hrk peptide (Hrk_G + 4A) harboring the LXXXGD motif augments its affinity by more than six-fold. Notably, of all the BH3 ligands analyzed here, Bad is the only one that contains a serine residue at the +4 position (S + 4) within the LXXXXD motif in lieu of an alanine or a glycine. To test how substitution of a serine at the +4 position with an alanine affects the binding of Bad to Bcl2, we introduced the S + 4A substitution into Bad peptide (Bad_S + 4A) harboring the LXXXSD motif and measured its binding to Bcl2. Our data show that the S + 4A substitution augments the binding of Bad peptide to Bcl2 by nearly 30-fold, implying that the serine residue cannot engage in close van der Waals contacts afforded by an alanine at the +4 position. Importantly, we also introduced the S + 4G substitution into Bad peptide (Bad_S + 4G) harboring the LXXXSD motif and measured its binding to Bcl2. Surprisingly, our analysis

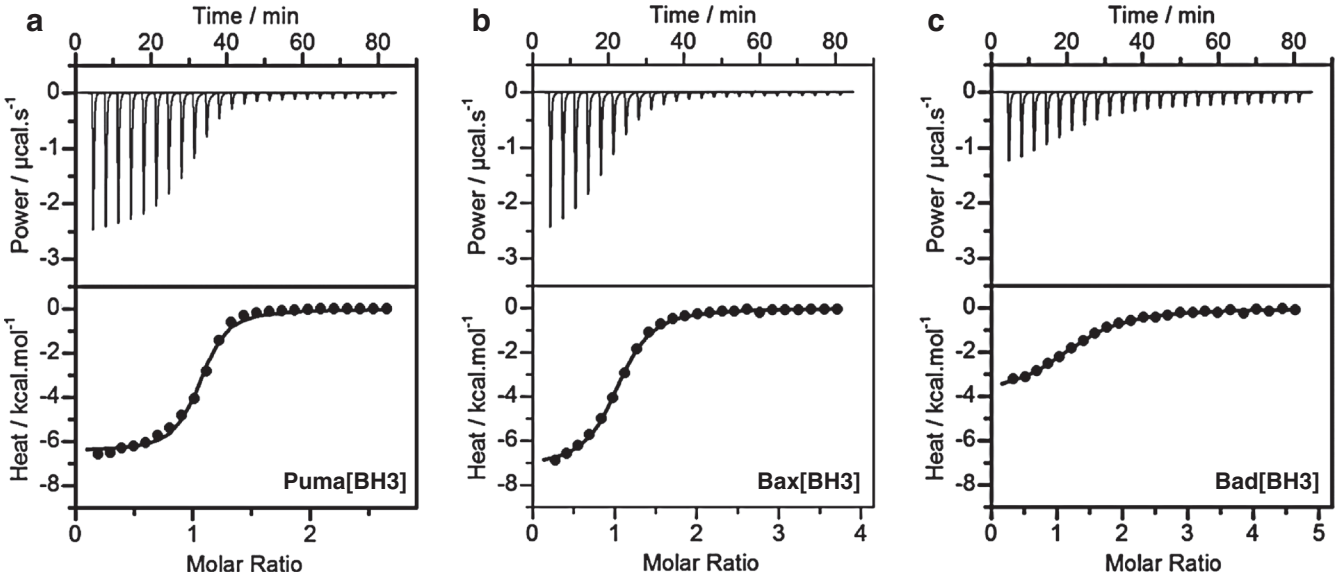

Figure 2. Representative isothermal titration calorimetry (ITC) isotherms for the binding of BH3 peptides of p53-upregulated modulator of apoptosis (Puma) (a), Bcl2-associated protein X (Bax) (b), and Bcl2-associated death promoter (Bad) (c) to Bcl2 in sodium phosphate buffer containing 100 mM NaCl at 25 °C and pH 7. Note that these BH3 peptides harbor LXXXAD (Puma), LXXXGD (Bax), and LXXXSD (Bad) motifs. The upper panels show raw ITC data expressed as change in thermal power with respect to time over the period of titration. In the lower panels, change in molar heat is expressed as a function of molar ratio of each BH3 peptide to B-cell lymphoma protein 2. The solid lines in the lower panels show non-linear least squares fit of data to a one-site binding model using ORIGIN as described previously (Wiseman *et al*., 1989; Bhat *et al*., 2012).

Journal of Molecular Recognition

Table 1. Thermodynamic parameters for the binding of various wildtype BH3 peptides to B-cell lymphoma protein 2 in sodium phosphate buffer containing 100 mM NaCl at 25 °C and pH 7

Peptide	Sequence	K_d (μM)	ΔH (kcal/mol)	TΔS (kcal/mol)	ΔG (kcal/mol)
Class I: LXXXAD motif					
Bmf	QAEVQIARK**L**QCI**AD**QFHRL	0.30 ± 0.07	−1.32 ± 0.05	+7.60 ± 0.11	−8.92 ± 0.16
Puma	QWAREIGAQ**L**RRM**AD**DLNAQ	0.37 ± 0.07	−6.57 ± 0.19	+2.22 ± 0.06	−8.79 ± 0.13
Class II: LXXX[G/S]D motif					
Bak	STMGQVG**R**Q**L**AII**GD**DINRR	1.30 ± 0.25	−10.91 ± 0.31	−2.86 ± 0.19	−8.04 ± 0.12
Bim	RPEIWIA**QE**L**R**RI**GD**EFNAY	1.45 ± 0.30	−0.94 ± 0.03	+7.04 ± 0.08	−7.97 ± 0.12
Bid	DIIRNIA**R**H**L**AQV**GD**SMDRS	2.10 ± 0.41	−4.52 ± 0.16	+3.23 ± 0.28	−7.75 ± 0.12
Bax	ASTKKLSES**L**KRI**GD**ELDSN	3.10 ± 0.66	−7.39 ± 0.19	+0.14 ± 0.06	−7.52 ± 0.13
Bik	EGSDALALR**L**ACI**GD**EMDVS	3.78 ± 0.79	−6.01 ± 0.07	+1.40 ± 0.05	−7.41 ± 0.13
Bad	WAAQRYG**R**E**L**RRM**SD**EFVDS	4.14 ± 0.80	−3.89 ± 0.07	+3.46 ± 0.04	−7.35 ± 0.12
Hrk	SAAQLTAAR**L**KAL**GD**ELHQR	25.02 ± 8.80	−1.29 ± 0.04	+5.01 ± 0.26	−6.30 ± 0.21
Noxa	ELEVECATQ**L**RRF**GD**KLNFR	NB	NB	NB	NB

Bmf, Bcl2-modifying factor; Puma, p53-upregulated modulator of apoptosis; Bak, Bcl2-homologous antagonist/killer; Bim, Bcl2-interacting mediator; Bid, BH3-interacting domain death agonist; Bax, Bcl2-associated protein X; Bik, Bcl2-interacting killer; Bad, Bcl2-associated death promoter; Hrk, harakiri apoptotic activator; Noxa, phorbol-induced protein 1.
Note that the BH3 peptides are divided into two classes on the basis of the consensus motif that they harbor. Absolutely conserved residues within the LXXXAD and LXXX[G/S]D are in bold. All parameters were obtained from isothermal titration calorimetry measurements. Errors were calculated from at least three independent measurements to one standard deviation. NB indicates no binding observed.

Table 2. Thermodynamic parameters for the binding of various mutant BH3 peptides to B-cell lymphoma protein 2 in sodium phosphate buffer containing 100 mM NaCl at 25 °C and pH 7

Peptide	Sequence	K_d (μM)	ΔH (kcal/mol)	TΔS (kcal/mol)	ΔG (kcal/mol)
Puma_A + 4G	QWAREIGAQ***L***RRM**GD**DLNAQ	2.12 ± 0.42	−8.10 ± 0.11	−0.34 ± 0.01	−7.75 ± 0.12
Hrk_G + 4A	SAAQLTAAR***L***KAL***AD***ELHQR	3.84 ± 0.71	−1.67 ± 0.08	+5.74 ± 0.18	−7.40 ± 0.12
Bad_S + 4A	WAAQRYGAE***L***RRM***AD***EFVDS	0.15 ± 0.03	−6.16 ± 0.16	+3.16 ± 0.04	−9.32 ± 0.11
Bad_S + 4G	WAAQRYGAE***L***RRM***GD***EFVDS	1.68 ± 0.38	−5.75 ± 0.05	+2.15 ± 0.18	−7.89 ± 0.14

Puma, p53-upregulated modulator of apoptosis; Hrk, harakiri apoptotic activator; Bad, Bcl2-associated death promoter.
Note that the absolutely conserved leucine and aspartate residues within the LXXXXD motif shared by all BH3 peptides are in bold italics, whereas the mutated residues within and flanking the LXXXXD motif are shown in bold for clarity. The nomenclature used for the relative positions of various residues is as described in Figure 1b. All parameters were obtained from isothermal titration calorimetry measurements. Errors were calculated from at least three independent measurements to one standard deviation.

reveals that the S + 4G substitution also augments the binding of Bad peptide to Bcl2, albeit by a little more than two-fold. This suggests that the serine residue at the +4 position within the Bad peptide harboring the LXXXSD motif is likely to be structurally destabilizing, presumably because of its relatively bulky hydroxyl sidechain compared with those of alanine and glycine. Alternatively, it is also plausible that the rather high conformational flexibility of glycine contributes favorably to the formation of Bcl2-Bad complex relative to serine at the +4 position.

In sum, our ITC analysis presented previously unequivocally demonstrates that the replacement of A + 4 residue within the LXXXAD motif to glycine results in the loss of binding energy as evidenced in the case of class II BH3 ligands harboring the LXXX[G/S]D motif.

Binding of BH3 ligands to B-cell lymphoma protein 2 is enthalpy-entropy compensated

Macromolecular interactions are often governed by enthalpy-entropy compensation phenomenon, whereby favorable enthalpic changes are largely compensated by unfavorable entropic factors, and vice versa, such that there is little or no gain in the overall free energy of binding (Lumry and Rajender, 1970; Starikov and Norden, 2007; Olsson *et al*., 2011). Importantly, the fact that the binding of BH3 ligands to Bcl2, with the exception of Bak peptide (Table 1), is predominantly driven by both favorable enthalpic ($\Delta H < 0$) and entropic ($T\Delta S > 0$) factors suggest that this protein-ligand interaction may override the enthalpy-entropy compensation phenomenon. However, our analysis reveals that the binding of both the class I (LXXXAD) and class II (LXXX[G/S]D) BH3 ligands to Bcl2 exquisitely obeys the enthalpy-entropy compensation phenomenon as evidenced by a slope of unity for the corresponding $T\Delta S - \Delta H$ plots (Figure 3a). Consistent with this observation, the corresponding ΔG displays little or negligible dependence on ΔH and TΔS (Figures 3b and 3c).

Structural models lend physical insights into the differential binding of various BH3 ligands to B-cell lymphoma protein 2

In order to uncover the physical basis of the differential binding of various BH3 ligands to Bcl2, we next modeled the structure of

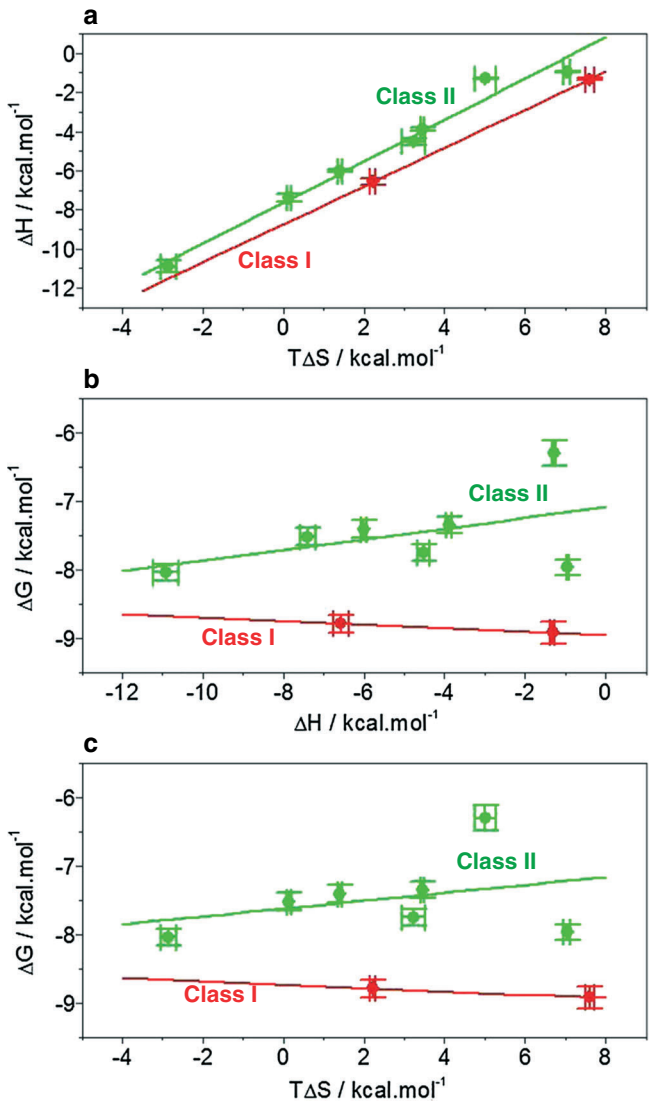

Figure 3. Inter-dependence of enthalpic (ΔH) and entropic (TΔS) contributions to the free energy (ΔG) for the binding of various BH3 peptides to B-cell lymphoma protein 2 in sodium phosphate buffer containing 100 mM NaCl at 25 °C and pH 7. (a) TΔS−ΔH plot. (b) ΔH−ΔG plot. (c) TΔS−ΔG plot. Note that the class I (red) and class II (green) BH3 ligands display distinct thermodynamic behaviors that can be grouped together as indicated by the linear fit of appropriate data points (solid lines). Error bars were calculated from at least three independent measurements to one standard deviation.

Bcl2 in complex with BH3 peptides harboring the LXXXAD (Puma), LXXXGD (Bax), and LXXXSD (Bad) motifs (Figure 4). Notably, Bcl2 is characterized by a central predominantly hydrophobic α-helical hairpin "dagger" (α5 and α6) surrounded by a "cloak" comprised of six amphipathic α-helices (α1–α4 and α7–α8) of varying lengths. It should also be noted here that the C-terminal region (residues 206–239) containing the TM domain (α9 helix) was not modeled into our structures for the sake of simplicity. Importantly, all three BH3 peptides derived from Puma, Bax, and Bad adopt an amphipathic α-helical conformation within the ligand binding groove—a shallow cleft formed by the juxtaposition of α2–α5 helices within Bcl2—in an almost indistinguishable fashion (Figures 4a–c). However, the differences between their binding modes surface at the level of amino acid residues within both the BH3 peptides and Bcl2 involved in the stabilization of these macromolecular complexes through specific intermolecular contacts. Thus, although the consensus L0 and D + 5 residues within the LXXXXD motif account for core intermolecular interactions between all three BH3 peptides and Bcl2, residues within and flanking this motif provide specificity and thereby account for their differential binding. Notably, although the benzyl ring of F153 located within the binding groove of Bcl2 appears to be oriented away from the aliphatic sidechain of L0 within each peptide, this does not seem to affect these two residues from engaging in close van der Waals contacts through the $H_3C\delta$ methyl sidechain atoms of L0 and the HCδ benzyl ring atoms of F153. In particular, although such van der Waals contacts are established between $H_3C\delta1$ methyl sidechain atoms of L0 and the HCδ2 benzyl ring atoms of F153 in the case of the binding of Puma peptide, the sidechain moieties of both of these residues adopt an alternative conformation in Bax and Bad peptides such that they rely on the $H_3C\delta2$ methyl sidechain atoms of L0 and the HCδ1 benzyl ring atoms of F153.

On the other hand, the interaction between the carboxylate sidechain of D + 5 within each peptide and the guanidine moiety of R146 within Bcl2 appears to be mediated via ion pairing and/or hydrogen bonding (Figures 4a–c). Of particular note is the observation that although the methyl sidechain of A + 4 within the LXXXAD motif of Puma participates in van der Waals contacts with the methyl sidechain of A149 in Bcl2, the G + 4 residue replacing the alanine residue within the LXXXGD motif of Bax cannot do so (Figures 4a and 4b). Accordingly, the van der Waals contact between A + 4 and A149 would be expected to favorably contribute to the free energy and thereby drive the binding of Puma and other BH3 ligands harboring the LXXXAD motif to Bcl2 with high affinity. In contrast, the absence of such intermolecular van der Waals contact between Bax as well as other BH3 ligands harboring the LXXXGD motif and Bcl2 could account for their rather weak binding relative to BH3 ligands harboring the LXXXAD motif in agreement with our thermodynamic data (Table 1). Interestingly, our structural model of Bad peptide in complex with Bcl2 reveals that the hydroxyl sidechain of S + 4 residue within the LXXXSD motif points away from the methyl sidechain of A149 and toward the aliphatic sidechain of R146 (Figure 4c). We believe that such orientation of S + 4 is likely to be structurally destabilizing. This notion is further supported by our thermodynamic data showing that the substitution of S + 4 with glycine within the LXXXSD motif augments the binding of Bad to Bcl2 by more than two-fold (Table 2).

Taken together, our structural models provide the physical basis for the binding of BH3 ligands harboring the LXXXAD motif to Bcl2 with high affinity, whereas those with the LXXX[G/S]D motif only afford weak interactions. Nonetheless, it is important to note that additional residues within and flanking the LXXXXD motif also participate in numerous key intermolecular contacts, thereby further contributing to the complexity of the molecular basis of Bcl2-ligand recognition.

The extent of surface burial poorly correlates with the free energy accompanying the binding of BH3 ligands to B-cell lymphoma protein 2

In an attempt to understand the contribution of polar and apolar residues involved in driving the Bcl2-ligand interactions, we next measured the dependence of enthalpic change (ΔH) associated

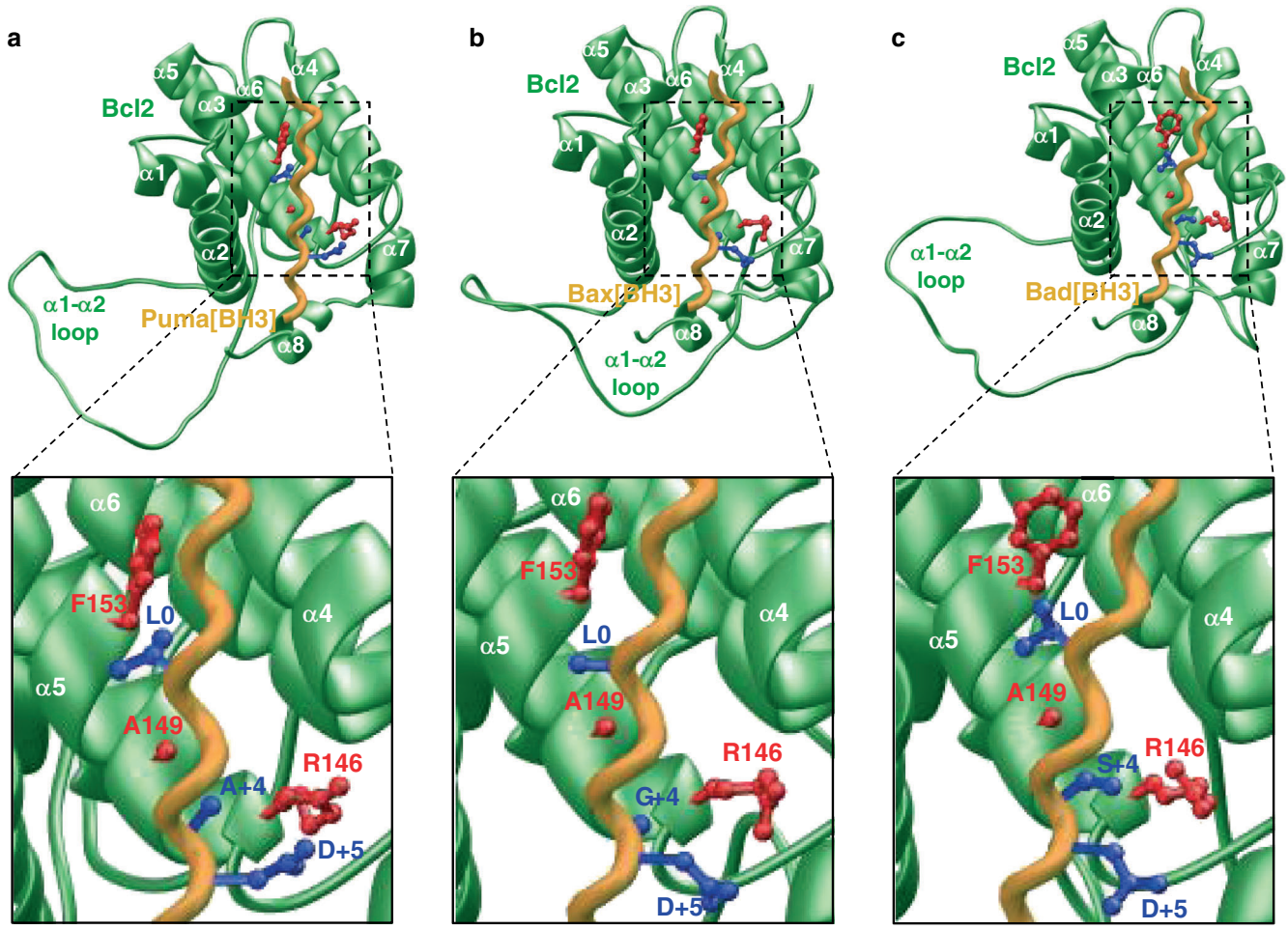

Figure 4. Structural models of B-cell lymphoma protein 2 bound to BH3 peptides of p53-upregulated modulator of apoptosis (Puma) (a), Bcl2-associated protein X (Bax) (b), and Bcl2-associated death promoter (Bad) (c). Note that these BH3 peptides harbor LXXXAD (Puma), LXXXGD (Bax), and LXXXSD (Bad) motifs. In each model, Bcl2 is shown in green, and the corresponding BH3 peptide is colored yellow. The expanded views show sidechain moieties of residues within Bcl2, and the corresponding BH3 peptide engaged in key intermolecular contacts in red and blue, respectively.

with the binding of various BH3 peptides to Bcl2 on temperature (Figure 5a). Importantly, the temperature dependence of ΔH is related to the change in heat capacity (ΔC_p) by Kirchhoff's relationship $\Delta C_p = d(\Delta H)/dT$, where T denotes temperature. Accordingly, ΔC_p accompanying the binding of various BH3 peptides to Bcl2 was determined from the corresponding slopes of $T-\Delta H$ plots (Figure 5a and Table 3). It is noteworthy that a negative value of ΔC_p was unanimously observed, implying that the binding of all BH3 peptides to Bcl2 is concomitant with the burial of predominantly apolar residues over polar groups. However, there appears to be little correlation between ΔC_p and the free energy (ΔG) of binding (Tables 1 and 3). Thus, for example, although high-affinity class I ligands display $-\Delta C_p$ values in the range 269–352 cal /mol/K, this largely overlaps with the range of 193–391 cal /mol/K observed for the low-affinity class II ligands.

In order to quantify how such differential changes in ΔC_p may reflect the extent of burial of polar and apolar surfaces upon the binding of various BH3 ligands to Bcl2, we also calculated the corresponding changes in SASA using empirically derived Eqs [3] and [4] (Murphy and Freire, 1992; Spolar and M.T. Record, 1994; Xie and Freire, 1994; Edgcomb and Murphy, 2000). As noted in Table 3, the change in apolar SASA ($\Delta SASA_{apolar}$) is on average about 50% greater than the corresponding change in polar SASA ($\Delta SASA_{polar}$) for the binding of each BH3 peptide to Bcl2. This implies that the hydrophobic forces play a dominant role in driving Bcl2-ligand interactions. Importantly, in agreement with ΔC_p values discussed previously, the change in total SASA ($\Delta SASA_{total}$) and ΔG appears to be poorly correlated (Figure 5b, top panel). Unsurprisingly, the lack of such a relationship also holds true for the underlying enthalpic (ΔH) and entropic ($T\Delta S$) components (Figure 5b, middle and bottom panels).

Binding of various BH3 ligands to B-cell lymphoma protein 2 is dominated by hydrophobic forces

Our data presented previously strongly suggest that hydrophobic forces and electrostatic contacts play an intricate role in mediating the Bcl2-ligand interactions. In an attempt to further elucidate such interplay between these forces, we next measured the effect of increasing NaCl concentration on the binding of BH3 peptides to Bcl2 (Figure 6). Our data show that although increasing salt concentration has little or negligible effect on the binding of high-affinity BH3 ligands such as Bmf and Puma harboring the LXXXAD motif (Figure 6a), the binding of those

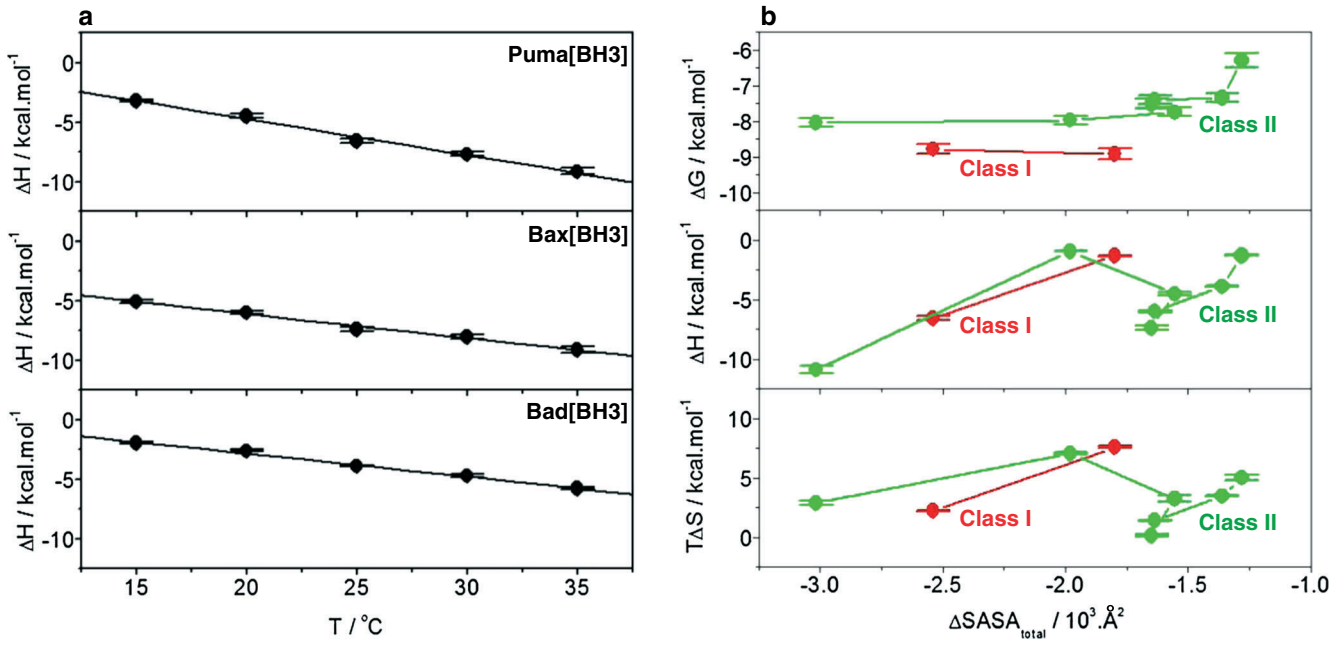

Figure 5. BH3 peptides undergo conformational changes upon binding to B-cell lymphoma protein 2 (Bcl2) in sodium phosphate buffer containing 100 mM NaCl at pH 7. (a) Dependence of enthalpy (ΔH) on temperature (T) for the binding of Bcl2 to BH3 peptides harboring LXXXAD (p53-upregulated modulator of apoptosis [Puma]), LXXXGD (Bcl2-associated protein X [Bax]), and LXXXSD (Bcl2-associated death promoter [Bad]) motifs. The solid lines through the data points represent linear fits. Error bars were calculated from at least three independent measurements to one standard deviation. (b) Dependence of free energy (ΔG) and the underlying enthalpic (ΔH) and entropic (TΔS) components on the total change in solvent-accessible surface area (SASA) ($\Delta SASA_{total}$) upon the binding of various BH3 peptides to Bcl2. Note that the class I (red) and class II (green) BH3 ligands display distinct thermodynamic behaviors that can be grouped together as indicated by the connecting of appropriate data points with solid lines. Error bars were calculated from at least three independent measurements to one standard deviation.

with the LXXX[G/S]D motif in general experiences a varying degree of enhancement (Figures 6a–c). Thus, whereas the binding of class II BH3 peptides of Bak, Bim, and Bid to Bcl2 appears to be largely independent of salt concentration in the 0–500 mM range in a manner akin to the binding of class I ligands, the binding of other class II ligands such as Bax, Bik, Bad, and Hrk is met with an enhancement of between two-to-five folds with increasing salt concentration. This salient observation is indicative of the fact that hydrophobic forces not only play a dominant but also a universal role in driving the Bcl2-BH3 interactions.

Importantly, our structural models suggest that the carboxyl moiety of D + 5 within each BH3 peptide likely engages in ion pairing and/or hydrogen bonding with the guanidine sidechain of R146 within Bcl2. It should be noted here that although salt disrupts the formation of ion pairs, it has little or negligible effect on hydrogen bonding interactions. Accordingly, we believe that the D + 5 and R146 residues are more

Table 3. Change in solvent-accessible surface area values determined from thermodynamic parameters for the binding of various wildtype BH3 peptides to B-cell lymphoma protein 2 in sodium phosphate buffer containing 100 mM NaCl at 25 °C and pH 7

Peptide	Sequence	ΔH_{60} (kcal/mol)	ΔC_p (kcal/mol/K)	$\Delta SASA_{polar}$ (Å^2)	$\Delta SASA_{apolar}$ (Å^2)	$\Delta SASA_{total}$ (Å^2)
Class I: LXXXAD motif						
Bmf	QAEVQIARK**L**QCI**AD**QFHRL	−11.30 ± 0.36	−0.269 ± 0.009	−666 ± 22	−1133 ± 38	−1800 ± 60
Puma	QWAREIGAQ**L**RRM**AD**DLNAQ	−18.41 ± 1.24	−0.352 ± 0.012	−1002 ± 57	−1538 ± 65	−2540 ± 122
Class II: LXXX[G/S]D motif						
Bak	STMGQVG**R**Q**L**AII**GD**DINRR	−24.25 ± 0.71	−0.391 ± 0.011	−1250 ± 36	−1768 ± 49	−3017 ± 84
Bim	RPEIWIA**QE**L**R**RI**GD**EFNAY	−11.93 ± 0.25	−0.302 ± 0.006	−720 ± 16	−1261 ± 26	−1981 ± 42
Bid	DIIRNIA**R**H**L**AQV**GD**SMDRS	−11.65 ± 0.18	−0.211 ± 0.002	−623 ± 9	−932 ± 12	−1555 ± 22
Bax	ASTKKLSES**L**KRI**GD**ELDSN	−14.20 ± 0.36	−0.203 ± 0.004	−707 ± 18	−942 ± 23	−1649 ± 40
Bik	EGSDALALR**L**ACI**GD**EMDVS	−13.38 ± 0.21	−0.209 ± 0.001	−684 ± 9	−952 ± 8	−1636 ± 18
Bad	WAAQRYG**RE**L**R**RM**SD**EFVDS	−10.18 ± 0.13	−0.185 ± 0.001	−545 ± 6	−816 ± 7	−1361 ± 13
Hrk	SAAQLTAAR**L**KAL**GD**ELHQR	−7.94 ± 0.35	−0.193 ± 0.005	−471 ± 18	−809 ± 25	−1281 ± 44

Bmf, Bcl2-modifying factor; Puma, p53-upregulated modulator of apoptosis; Bak, Bcl2-homologous antagonist/killer; Bim, Bcl2-interacting mediator; Bid, BH3-interacting domain death agonist; Bax, Bcl2-associated protein X; Bik, Bcl2-interacting killer; Bad, Bcl2-associated death promoter; Hrk, harakiri apoptotic activator.
Errors were calculated from at least three independent measurements to one standard deviation.

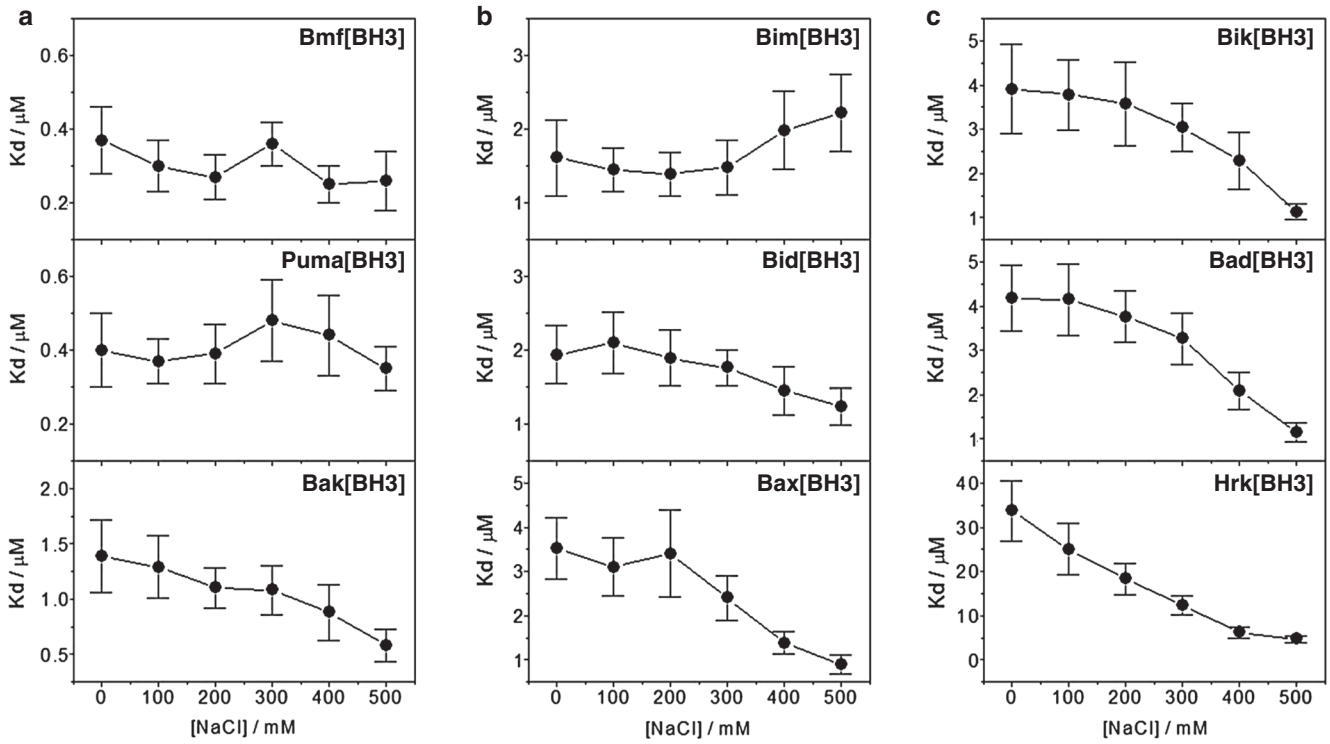

Figure 6. Effect of NaCl concentration on the binding, as measured by the binding constant (K_d), of B-cell lymphoma protein 2 to various BH3 peptides harboring LXXXAD and LXXX[G/S]D motifs in sodium phosphate buffer at 25 °C and pH 7. Note that the solid lines are used to connect various data points for clarity. Error bars were calculated from at least three independent measurements to one standard deviation.

likely to be involved in the formation of intermolecular hydrogen bonding for the binding of Bax, Bik, Bad, and Hrk, although they are more likely to participate in the formation of intermolecular salt bridges in the case of Bmf, Puma, Bak, Bim, and Bid. This could in part account for the observation that increasing salt concentration affects the binding of various BH3 peptides to Bcl2 in a differential manner. On the other hand, differences in the nature of amino acids within and flanking the core LXXXXD motif are also likely to contribute to the precise mechanism that the various BH3 peptides employ in binding to Bcl2.

Molecular dynamics sheds light on the structural stability and motional properties of various B-cell lymphoma protein 2-ligand complexes

In an attempt to understand and compare the structural stability and conformational flexibility of various Bcl2-ligand complexes, we conducted MD simulations on the modeled structures of Bcl2 bound to BH3 peptides harboring the LXXXAD (Puma), LXXXGD (Bax), and LXXXSD (Bad) motifs over tens of nanoseconds (Figure 7). As shown in Figure 7a, the MD trajectories reveal that although all three Bcl2-peptide complexes asymptotically reach structural equilibrium after about 50 ns with an overall root mean square deviation (RMSD) oscillating between 8–10 Å, there are subtle dynamic differences. This implies that although all three complexes harbor internal regions of relatively high flexibility, the exact nature of such fluctuations is likely to be somewhat different within each complex. To understand the origin of such structural fluctuations, we next deconvoluted the overall RMSD of the three complexes into their individual protein and peptide constituent components. Our analysis shows that both Bcl2 and BH3 peptides display relatively low structural stability. Thus, although an RMSD for Bcl2 is comparable with that of the corresponding protein-peptide complex, the BH3 peptides also display a rather high RMSD hovering between 2–3 Å at equilibrium. Given that the BH3 peptides merely span a stretch of 20 residues, an RMSD of greater than 2 Å is indicative of the fact that the starting structure undergoes significant deviation during the course of the simulations. In particular, the Bax and Bad peptides show much lower stability in complex with Bcl2 compared with Puma, which remarkably correlates with their respective binding affinities (Table 1).

An alternative means to assess mobility and stability of macromolecular complexes is through an assessment of the root mean square fluctuation of specific atoms over the entire course of MD simulations. Figures 7b and 7c provide such analysis for the backbone atoms of each residue within the corresponding Bcl2 and peptide components of all three complexes. Interestingly, although most residues appear to be highly ordered within Bcl2 across all three complexes (Figure 7b), there are also notable differences in the dynamics of specific regions. In particular, although the N-termini of Bcl2 within all three complexes harbor high mobility, the same does not hold true in the case of the C-terminus—the mobility of which exquisitely correlates with the binding of affinity of the corresponding peptides (Table 1). Thus, although the C-terminus of Bcl2 is highly ordered in the case of the high-affinity Puma peptide, it becomes increasingly more mobile with decreasing affinities displayed by Bax and Bad. Additionally, subtle differences in the mobility of residues located within the α1–α2 loop of

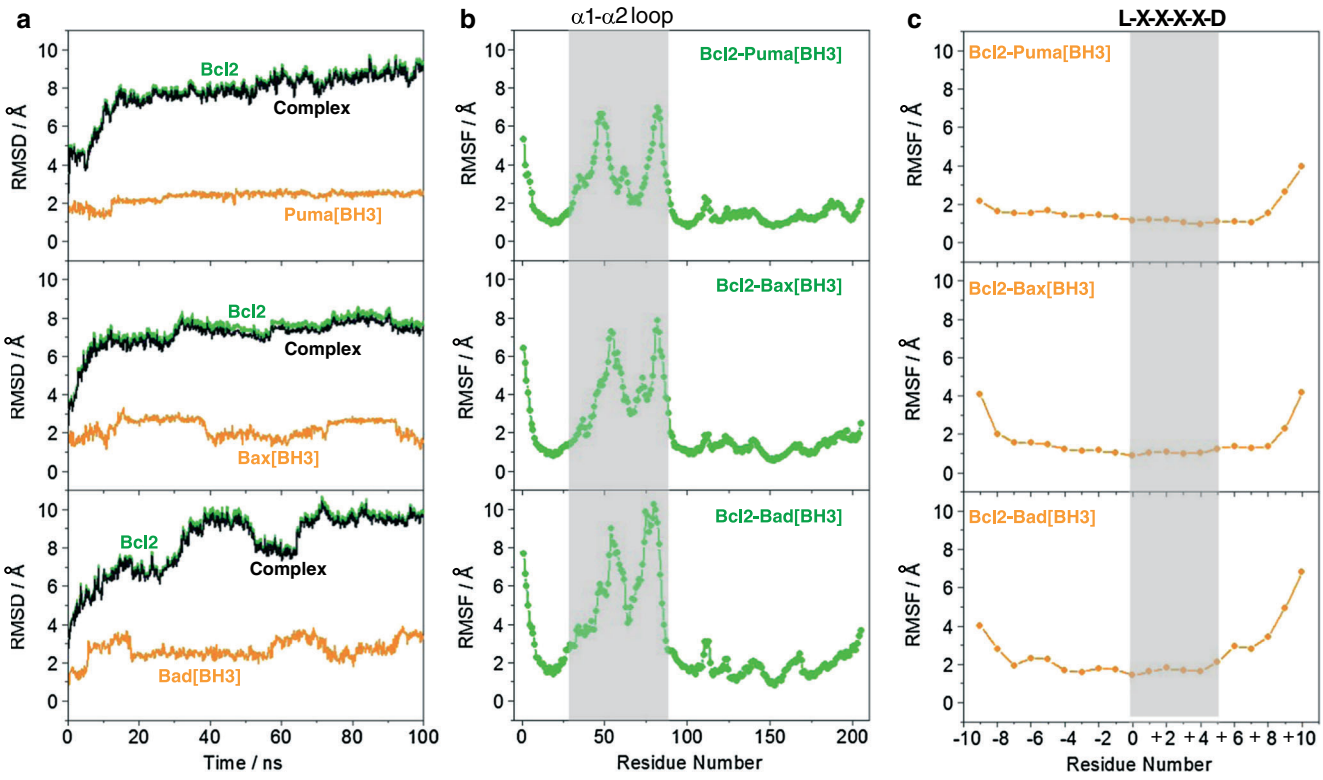

Figure 7. Root mean square deviation (RMSD) and fluctuation (RMSF) of backbone atoms (N, Cα, and C) obtained from MD analysis on the structural models of B-cell lymphoma protein 2 (Bcl2) bound to various BH3 peptides harboring LXXXAD (p53-upregulated modulator of apoptosis [Puma]), LXXXGD (Bcl2-associated protein X [Bax]), and LXXXSD (Bcl2-associated death promoter [Bad]) motifs. (a) RMSD of backbone atoms within each simulated structure relative to the initial modeled structure of Bcl2 bound to BH3 peptides of Puma (top panel), Bax (middle panel), and Bad (bottom panel) for the corresponding Bcl2-peptide complex (black), Bcl2 alone (green), and BH3 peptide alone (yellow) as a function of simulation time. (b) RMSF of backbone atoms averaged over the entire course of corresponding MD trajectory of Bcl2 bound to BH3 peptides of Puma (top panel), Bax (middle panel), and Bad (bottom panel) as a function of residue number within Bcl2. The shaded vertical rectangular box denotes residues located within the α1–α2 loop. (c) RMSF of backbone atoms averaged over the entire course of corresponding MD trajectory of Bcl2 bound to BH3 peptides of Puma (top panel), Bax (middle panel), and Bad (bottom panel) as a function of residue number within each peptide. The shaded vertical rectangular box denotes residues located within the LXXXXD motif.

Bcl2 bound to each of the three BH3 peptides are also apparent. On the other hand, there are also important differences in the conformational flexibility of residues within and flanking the core LXXXXD motif of BH3 peptides within all three complexes (Figure 7c). Of particular note is the observation that although N-terminus of high-affinity Puma peptide displays relatively high stability, the N-termini of low-affinity Bax and Bad peptides are relatively less stable. Moreover, although the C-termini of all three BH3 peptides appear to be highly mobile, such mobility is evidently more pronounced in the case of Bad peptide. Notably, residues within the LXXXXD motif also show greater mobility in Bad peptide compared with the corresponding residues within the other two peptides.

Taken together, these observations are in a remarkable agreement with our thermodynamic and structural analysis showing that the A + 4 residue within the LXXXXD motif substantially contributes to the stability of Bcl2-BH3 complexes (Table 1 and Figure 4). Additionally, the MD simulations presented previously are also consistent with the notion that the substitution of S + 4 with glycine within the LXXXSD motif not only augments the binding of Bad to Bcl2 by more than two-fold but that the S + 4 residue is also likely to be structurally destabilizing compared with glycine (Table 2 and Figure 4c).

Differential stability of specific pairs of intermolecular contacts underscores the formation of various B-cell lymphoma protein 2-ligand complexes

Our structural models suggest that although the consensus L0 and D + 5 residues within the LXXXXD motif provide the core intermolecular contacts with specific residues lining the hydrophobic groove within Bcl2, the residue located at the +4 position appears to be a major determinant of the differential binding of BH3 peptides harboring the LXXXAD (Puma), LXXXGD (Bax), and LXXXSD (Bad) motifs (Figure 4). In order to further corroborate this notion and to test the stability of these intermolecular contacts, we compared the changes in distance between specific pairs of atoms within each of the three complexes as a function of simulation time from our MD analysis (Figure 8). Notably, although the distance between Cδ benzyl ring atoms of F153 (F153.Cδ1/δ2) within Bcl2 and Cδ methyl atoms of L0 (L0.Cδ1/δ2) within the high-affinity Puma peptide remains more or less constant at around 4 Å throughout the simulation (Figure 8a), it appears to be more fluctuating with an equilibrium value of close to 6 Å in the case of complexes with low-affinity Bax and Bad peptides. This implies that although the van der Waals contact between the benzyl ring of F153 and the aliphatic sidechain of L0 is a point of relatively high stability between Bcl2 and the Puma

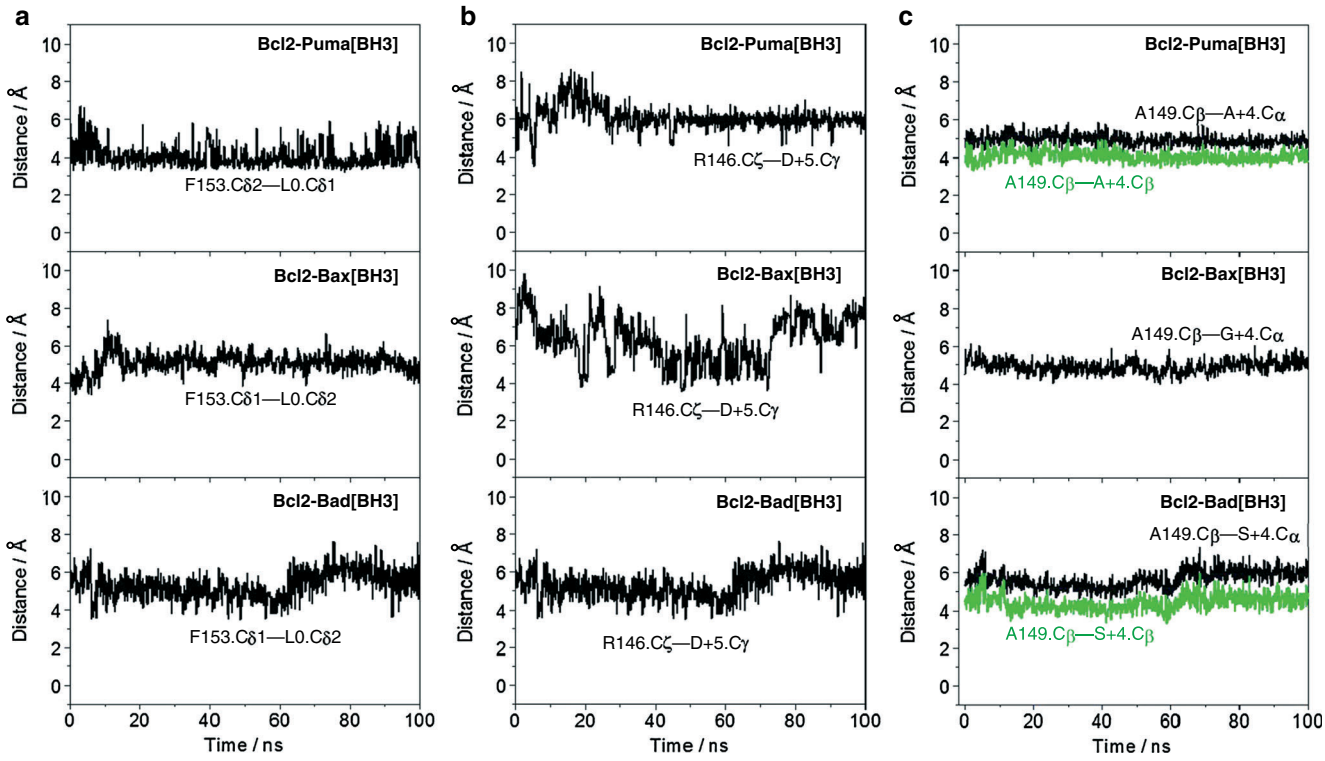

Figure 8. Inter-atomic distances obtained from molecular dynamics analysis on the structural models of B-cell lymphoma protein 2 (Bcl2) bound to various BH3 peptides harboring LXXXAD (Puma [p53-upregulated modulator of apoptosis]), LXXXGD (Bax [Bcl2-associated protein X]), and LXXXSD (Bad [Bcl2-associated death promoter]) motifs. (a) Distance between Cδ benzyl ring atoms of F153 (F153.Cδ1/δ2) within Bcl2 and Cδ methyl atoms of L0 (L0.Cδ1/δ2) within the BH3 peptides of Puma (top panel), Bax (middle panel), and Bad (bottom panel) as a function of simulation time (black). (b) Distance between Cζ atom of R146 (R146.Cζ) within Bcl2 and Cγ atom of D + 5 (D + 5.Cγ) within the BH3 peptides of Puma (top panel), Bax (middle panel), and Bad (bottom panel) as a function of simulation time (black). (c) Distances between Cβ atom of A149 (A149.Cβ) within Bcl2 and Cα atom of X + 4 (X + 4.Cα) within the BH3 peptides of Puma (top panel), Bax (middle panel), and Bad (bottom panel) as a function of simulation time (black), or between Cβ atom of A149 (A149.Cβ) within Bcl2 and Cβ atom of X + 4 (X + 4.Cβ) within the BH3 peptides of Puma (top panel) and Bad (bottom panel) as a function of simulation time (green). Note that X + 4 is, respectively, alanine, glycine, and serine within the BH3 peptides of Puma, Bax, and Bad.

peptide, this intermolecular interaction is strikingly less stable for complexes with the low-affinity peptides. In a likewise manner, the intermolecular contact between R146 in Bcl2 and D + 5 within the BH3 peptides shows higher stability in the case of Puma peptide compared with Bax and Bad (Figure 8b). Thus, although the distance between Cζ atom of R146 (R146.Cζ) and Cγ atom of D + 5 (D + 5.Cγ) within the Puma peptide attains a highly stable equilibrium value of 6 Å, it displays much higher fluctuations in the case of the other two peptides. This strongly argues that the ion pairing and/or hydrogen bonding interaction between the guanidine moiety of R146 and the carboxyl moiety of D + 5 is likely to be more stable in the formation of a complex between Bcl2 and the Puma peptide compared with the complexes with Bax and Bad peptides.

Consistent with the differential stability of F153-L0 and R146-D + 5 intermolecular contacts in the formation of complexes of Bcl2 with various BH3 peptides observed previously (Figures 8a and 8b), the behavior of the A149-A + 4 contact as a function of simulation time further reinforces this continuing trend (Figure 8c). Thus, although the distance between Cβ atom of A149 (A149.Cβ) within Bcl2 and Cα atom of X + 4 residue (X + 4.Cα) within Puma peptide displays relatively high stability, it appears to be somewhat more fluctuating in the case of Bax and Bad peptides. Our thermodynamic data and structural models suggest that the substitution of S + 4 with glycine within the LXXXSD motif not only augments the binding of Bad to Bcl2 by more than two-fold but that the S + 4 residue is also likely to be structurally destabilizing compared with glycine (Table 2 and Figure 4c). Consistent with this observation, the distance between Cβ atom of A149 (A149.Cβ) within Bcl2 and Cβ atom of X + 4 residue (X + 4.Cβ) within Puma peptide displays higher stability than the corresponding distance in the Bcl2-Bad complex.

In sum, our MD analysis presented previously strongly argues that the van der Waals contact between the methyl sidechains of A149 and A + 4 does not only plays a key role in driving the binding of Bcl2 to BH3 ligands harboring the LXXXAD motif with high affinity but its stabilizing effect may also allosterically contribute to the stability of neighboring intermolecular contacts, particularly those involving the residues located at the 0 and +5 positions within the BH3 peptides. Although an exhaustive analysis of all specific pairs of atoms that engage in key intermolecular contacts between Bcl2 and BH3 peptides is beyond the scope of this work, we nonetheless note that the Bcl2-ligand interactions are further buttressed by an extensive network of intermolecular contacts between numerous residues—in addition to those discussed previously—within and flanking the LXXXXD motif of BH3 peptides with those located in the binding groove of Bcl2.

CONCLUSIONS

Although differential binding of various BH3 ligands to Bcl2 apoptotic repressor is well-documented (Petros *et al.*, 2001;

Petros *et al*., 2004; Ku *et al*., 2011; London *et al*., 2012), our study provides detailed biophysical insights into the molecular basis of a key recognition event involved in mediating apoptosis. It is noteworthy that the protein construct employed here to interrogate the binding specificity and promiscuity of Bcl2 toward its BH3 ligands was devoid of the C-terminal TM domain. This was highly desirable given that the TM domain has been shown to exert an inhibitory role by virtue of its ability to competitively bind to the canonical hydrophobic groove within apoptotic repressors, which is also shared by BH3 ligands (Denisov *et al*., 2003; Hinds *et al*., 2003; Bhat *et al*., 2012). Accordingly, the use of fully intact Bcl2—not to mention that efforts in our laboratory and those of others have hitherto met with no success to purify this full-length construct to sufficient quantities and apparent homogeneity for subsequent biophysical analysis—would have rendered it technically challenging to study the BH3 ligands, which bind with weak affinity. On the same token, the use of short 20-mer BH3 peptides to mimic the action of various BH3 ligands was also necessary because their activation usually requires post-translational cleavage or modification *in vivo*. For example, Bid is cleaved by caspases to generate an active fragment containing the BH3 domain (tBid)(Li *et al*., 1998), whereas full-length Bad displays poor affinity toward Bcl2 and BclXL *in vitro* (unpublished observations). We also note that we did not observe the binding of Noxa peptide to Bcl2 even when we varied the temperature, buffer, or solution pH. Surprisingly, a recent report argues in support of a high-affinity interaction between Bcl2 and full-length Noxa (Smith *et al*., 2011). In light of this finding, it seems most probable that residues flanking the 20-residue BH3 peptide of Noxa are absolutely required for its binding to Bcl2.

Notwithstanding these limitations, our biophysical analysis suggests that the various BH3 ligands of Bcl2 can be divided into two distinct classes harboring the LXXXAD (class I) and LXXX[G/S]D motifs on the basis of their binding characteristics. Thus, whereas class I BH3 ligands recognize Bcl2 with high affinity in the submicromolar range, class II ligands afford rather weak interactions. Importantly, our analysis also reveals that the binding of both class I and II ligands to Bcl2 is subject to the enthalpy-entropy compensation phenomenon, implying that the design of novel anti-Bcl2 inhibitors is likely to encounter a thermodynamic bottleneck. On the other hand, although increasing ionic strength has little or negligible effect on the binding of high-affinity BH3 ligands harboring the LXXXAD motif, the binding of those with the LXXX[G/S]D motif in general experiences a varying degree of enhancement. This salient observation is indicative of the fact that hydrophobic forces not only play a dominant but also a universal role in driving the Bcl2-BH3 interactions.

On the basis of the data presented above, we believe that whereas class I BH3 ligands likely represent the most potent inhibitors of Bcl2 *in vivo*, class II ligands are likely to be promiscuous partners of Bcl2 as they may target other apoptotic repressors such as Bcl2, BclW, Mcl1, and Bfl1. Toward this goal, our future studies will set out to address the specificity of various BH3 ligands and their cross-reactivity toward these apoptotic repressors. In short, our study provides new biophysical insights into understanding the binding promiscuity of Bcl2 toward its BH3 ligands and thus lays the foundation for uncovering the complexity of the molecular events involved in mediating the specificity of various Bcl2 members toward each other.

Acknowledgements

This work was supported by the National Institutes of Health grants R01-GM083897 and funds from the USylvester Braman Family Breast Cancer Institute (to AF). CBM is a recipient of a post-doctoral fellowship from the National Institutes of Health (award# T32-CA119929).

REFERENCES

Adams JM, Cory S. 1998. The Bcl-2 protein family: arbiters of cell survival. *Science* **281**: 1322–1326.

Berendsen HJC, Grigera JR, Straatsma TP. 1987. The missing term in effective pair potentials. *J Phys Chem* **91**: 6269–6271.

Bhat V, McDonald CB, Mikles DC, Deegan BJ, Seldeen KL, Bates ML, Farooq A. 2012. Ligand binding and membrane insertion compete with oligomerization of the BclXL apoptotic repressor. *J. Mol. Biol.* **416**: 57–77.

Boersma MD, Sadowsky JD, Tomita YA, Gellman SH. 2008. Hydrophile scanning as a complement to alanine scanning for exploring and manipulating protein–protein recognition: application to the Bim BH3 domain. *Protein Sci.* **17**: 1232–1240.

Carson M. 1991. Ribbons 2.0. *J. Appl. Crystallogr.* **24**: 958–961.

Chipuk JE, Green DR. 2008. How do BCL-2 proteins induce mitochondrial outer membrane permeabilization? *Trends Cell Biol.* **18**: 157–164.

Chipuk JE, Fisher JC, Dillon CP, Kriwacki RW, Kuwana T, Green DR. 2008. Mechanism of apoptosis induction by inhibition of the anti-apoptotic BCL-2 proteins. *Proc Natl Acad Sci U S A* **105**: 20327–20332.

Chipuk JE, Moldoveanu T, Llambi F, Parsons MJ, Green DR. 2010. The BCL-2 family reunion. *Mol. Cell* **37**: 299–310.

Darden TA, York D, Pedersen L. 1993. Particle mesh Ewald: an N.log(N) method for Ewald sums in large systems. *J. Chem. Phys.* **98**: 10089–10092.

Dejean LM, Ryu SY, Martinez-Caballero S, Teijido O, Peixoto PM, Kinnally KW. 2010. MAC and Bcl-2 family proteins conspire in a deadly plot. *Biochim. Biophys. Acta* **1797**: 1231–1238.

Del Bufalo D, Biroccio A, Leonetti C, Zupi G. 1997. Bcl-2 overexpression enhances the metastatic potential of a human breast cancer line. *FASEB J.* **11**; 947–953.

Denisov AY, Madiraju MS, Chen G, Khadir A, Beauparlant P, Attardo G, Shore GC, Gehring K. 2003. Solution structure of human BCL-w: modulation of ligand binding by the C-terminal helix. *J. Biol. Chem.* **278**: 21124–21128.

Dewson G, Kluck RM. 2009. Mechanisms by which Bak and Bax permeabilise mitochondria during apoptosis. *J. Cell Sci.* **122**: 2801–2808.

Dutta S, Gulla S, Chen TS, Fire E, Grant RA, Keating AE. 2010. Determinants of BH3 binding specificity for Mcl-1 versus Bcl-xL. *J. Mol. Biol.* **398**; 747–762.

Edgcomb SP, Murphy KP. 2000. Structural energetics of protein folding and binding. *Curr. Opin. Biotechnol.* **11**: 62–66.

Espana L, Fernandez Y, Rubio N, Torregrosa A, Blanco J, Sierra A. 2004. Overexpression of Bcl-xL in human breast cancer cells enhances organ-selective lymph node metastasis. *Breast Cancer Res. Treat.* **87**: 33–44.

Gasteiger E, Hoogland C, Gattiker A, Duvaud S, Wilkins MR, Appel RD, Bairoch A. 2005. Protein identification and analysis tools on the ExPASy server. In The proteomics protocols handbook, JM Walker (ed.). Humana Press: Totowa, New Jersey, USA; 571–607.

van der Goot FG, Gonzalez-Manas JM, Lakey JH, Pattus F. 1991. A 'molten-globule' membrane-insertion intermediate of the pore-forming domain of colicin A. *Nature* **354**: 408–410.

Gross A, McDonnell JM, Korsmeyer SJ. 1999. BCL-2 family members and the mitochondria in apoptosis. *Genes Dev.* **13**: 1899–1911.

Hess B. 2008. GROMACS 4: algorithms for highly efficient, load-balanced, and scalable molecular simulation. *J. Chem. Theory. Comput.* **4**: 435–447.

Hess B, Bekker H, Berendsen HJC, Fraaije JGEM. 1997. LINCS: a linear constraint solver for molecular simulations. *J. Comput. Chem.* **18**: 1463–1472.

Hinds MG, Lackmann M, Skea GL, Harrison PJ, Huang DC, Day CL. 2003. The structure of Bcl-w reveals a role for the C-terminal residues in modulating biological activity. *EMBO J.* **22**: 1497–1507.

Huang DC, Strasser A. 2000. BH3-only proteins-essential initiators of apoptotic cell death. *Cell* **103**: 839–842.

Jorgensen WL, Tirado-Rives J. 1988. The OPLS force field for proteins: energy minimizations for crystals of cyclic peptides and crambin. *J. Am. Chem. Soc.* **110**: 1657–1666.

Kaminski GA, Friesner RA, Tirado-Rives J, Jorgensen WL. 2001. Evaluation and reparametrization of the OPLS-AA force field for proteins via comparison with accurate quantum chemical calculations on peptides. *J. Phys. Chem. B* **105**: 6474–6487.

Korsmeyer SJ. 1999. BCL-2 gene family and the regulation of programmed cell death. *Cancer Res.* **59**: 1693s–1700s.

Ku B, Liang C, Jung JU, Oh BH. 2011. Evidence that inhibition of BAX activation by BCL-2 involves its tight and preferential interaction with the BH3 domain of BAX. *Cell Res.* **21**; 627–641.

Kuwana T, Newmeyer DD. 2003. Bcl-2-family proteins and the role of mitochondria in apoptosis. *Curr. Opin. Cell Biol.* **15**: 691–699.

Lakey JH, van der Goot FG, Pattus F. 1994. All in the family: the toxic activity of pore-forming colicins. *Toxicology* **87**: 85–108.

Lee EF, Czabotar PE, Smith BJ, Deshayes K, Zobel K, Colman PM, Fairlie WD. 2007. Crystal structure of ABT-737 complexed with Bcl-xL: implications for selectivity of antagonists of the Bcl-2 family. *Cell Death Differ.* **14**: 1711–1713.

Li H, Zhu H, Xu CJ, Yuan J. 1998. Cleavage of BID by caspase 8 mediates the mitochondrial damage in the Fas pathway of apoptosis. *Cell* **94**; 491–501.

Liu X, Dai S, Zhu Y, Marrack P, Kappler JW. 2003. The structure of a Bcl-xL/Bim fragment complex: implications for Bim function. *Immunity* **19**: 341–352.

London E. 1992. Diphtheria toxin: membrane interaction and membrane translocation. *Biochim. Biophys. Acta* **1113**: 25–51.

London N, Gulla S, Keating AE, Schueler-Furman O. 2012. In silico and in vitro elucidation of BH3 binding specificity toward Bcl-2. *Biochemistry* **51**: 5841–5850.

Lumry R, Rajender S. 1970. Enthalpy-entropy compensation phenomena in water solutions of proteins and small molecules: a ubiquitous property of water. *Biopolymers* **9**: 1125–1227.

Marti-Renom MA, Stuart AC, Fiser A, Sanchez R, Melo F, Sali A. 2000. Comparative protein structure modeling of genes and genomes. *Annu. Rev. Biophys. Biomol. Struct.* **29**: 291–325.

Moroy G, Martin E, Dejaegere A, Stote RH. 2009. Molecular basis for Bcl-2 homology 3 domain recognition in the Bcl-2 protein family: identification of conserved hot spot interactions. *J. Biol. Chem.* **284**: 17499–17511.

Murphy KP, Freire E. 1992. Thermodynamics of structural stability and cooperative folding behavior in proteins. *Adv. Protein Chem.* **43**: 313–361.

Olsson TS, Ladbury JE, Pitt WR, Williams MA. 2011. Extent of enthalpy-entropy compensation in protein-ligand interactions. *Protein Sci.* **20**: 1607–1618.

Petros AM, Nettesheim DG, Wang Y, Olejniczak ET, Meadows RP, Mack J, Swift K, Matayoshi ED, Zhang H, Thompson CB, Fesik SW. 2000. Rationale for Bcl-xL/Bad peptide complex formation from structure, mutagenesis, and biophysical studies. *Protein Sci.* **9**: 2528–2534.

Petros AM, Medek A, Nettesheim DG, Kim DH, Yoon HS, Swift K, Matayoshi ED, Oltersdorf T, Fesik SW. 2001. Solution structure of the antiapoptotic protein bcl-2. *Proc Natl Acad Sci U S A* **98**: 3012–3017.

Petros AM, Olejniczak ET, Fesik SW. 2004. Structural biology of the Bcl-2 family of proteins. *Biochim. Biophys. Acta* **1644**; 83–94.

Placzek WJ, Wei J, Kitada S, Zhai D, Reed JC, Pellecchia M. 2010. A survey of the anti-apoptotic Bcl-2 subfamily expression in cancer types provides a platform to predict the efficacy of Bcl-2 antagonists in cancer therapy. *Cell Death Dis.* **1**: e40.

Sattler M, Liang H, Nettesheim D, Meadows RP, Harlan JE, Eberstadt M, Yoon HS, Shuker SB, Chang BS, Minn AJ, Thompson CB, Fesik SW. 1997. Structure of Bcl-xL-Bak peptide complex: recognition between regulators of apoptosis. *Science* **275**: 983–986.

Schendel SL, Montal M, Reed JC. 1998. Bcl-2 family proteins as ion-channels. *Cell Death Differ.* **5**: 372–380.

Smith AJ, Dai H, Correia C, Takahashi R, Lee SH, Schmitz I, Kaufmann SH. 2011. Noxa/Bcl-2 protein interactions contribute to bortezomib resistance in human lymphoid cells. *J. Biol. Chem.* **286**: 17682–17692.

Spolar RS, M.T. Record J. 1994. Coupling of local folding to site-specific binding of proteins to DNA. *Science* **263**: 777–784.

Starikov EB, Norden B. 2007. Enthalpy-entropy compensation: a phantom or something useful? *J. Phys. Chem. B* **111**: 14431–14435.

Toukan K, Rahman A. 1985. Molecular-dynamics study of atomic motions in water. *Physical Review B* **31**: 2643–2648.

Van Der Spoel D, Lindahl E, Hess B, Groenhof G, Mark AE, Berendsen HJ. 2005. GROMACS: fast, flexible, and free. *J. Comput. Chem.* **26**: 1701–1718.

Wiseman T, Williston S, Brandts JF, Lin LN. 1989. Rapid measurement of binding constants and heats of binding using a new titration calorimeter. *Anal. Biochem.* **179**: 131–137.

Xie D, Freire E. 1994. Molecular basis of cooperativity in protein folding. V. Thermodynamic and structural conditions for the stabilization of compact denatured states. *Proteins* **19**: 291–301.

Yao Y, Bobkov AA, Plesniak LA, Marassi FM. 2009. Mapping the interaction of pro-apoptotic tBID with pro-survival BCL-XL. *Biochemistry* **48**: 8704–8711.

Zakharov SD, Cramer WA. 2002. Colicin crystal structures: pathways and mechanisms for colicin insertion into membranes. *Biochim. Biophys. Acta* **1565**: 333–346.